A Finite-Difference Method for Transonic Airfoil Design

JOSEPH L. STEGER* AND JOHN M. KLINEBERG*
NASA Ames Research Center, Moffett Field, Calif.

This paper describes an inverse method for designing transonic airfoil sections or for modifying existing profiles. Mixed finite-difference procedures are applied to the equations of transonic small disturbance theory to determine the airfoil shape corresponding to a given surface pressure distribution. The equations are solved for the velocity components in the physical domain, and flows with embedded shock waves can be calculated. To facilitate airfoil design, the method allows alternating between inverse and direct calculations to obtain a profile shape that satisfies given geometric constraints. Examples are shown of the application of the technique to improve the performance of several lifting airfoil sections. The extension of the method to three dimensions for designing supercritical wings is also indicated.

I. Introduction

In a series of papers beginning in 1964, Nieuwland and his coworkers (e.g., Ref. 1) extended Lighthill's earlier application of hodograph methods to calculate shock-free supercritical flow about a family of quasi-elliptical airfoils. By systematically varying seven independent parameters, almost symmetrical profiles with nose camber were obtained. Several of these airfoils were tested in the NLR transonic tunnel (e.g., Ref. 2) and showed good agreement with the theory, although differences over the aft portion of the airfoil (probably caused by boundary-layer effects) resulted in a 20% decrease in lift at optimum conditions. This loss in lift could be partially recovered by introducing a small amount of rear camber, through the deflection of a trailing-edge flap, without greatly modifying the drag characteristics.

More recently, Garabedian and Korn[3] have developed an efficient hodograph technique that involves analytic continuation of the partial differential equations into the complex plane. Their method also requires specifying seven parameters, but it is more general than Nieuwland's approach and has been used to design useful, highly cambered, shock-free supercritical airfoils. Experiments conducted in the NRC high Reynolds-number facility by Kacprzynski et al.[4] again showed good agreement with the theory, provided small corrections for Mach number and angle of attack were made.

Hodograph techniques have therefore proved to be practical methods for supercritical airfoil design, although they contain several inherent disadvantages. One of the difficulties is that the methods require complicated input or initial conditions, such as the Mach number and flow angle at the profile trailing edge for Nieuwland's theory, or a set of logarithmic terms giving singularities inside the airfoil for Korn's approach. This is a particular disadvantage when profile modification is attempted. A second limitation of the hodograph methods is that they are restricted to shock-free solutions, and for certain applications, at least, the optimum airfoil will not be shockless. This is because weak shock waves do not generate appreciable wave drag and do not cause separation of a fully developed turbulent boundary layer. At the same time, a transonic airfoil with a weak recompression shock could have considerably more lift than one that is shock free, could be designed for a higher freestream Mach number, and could have less variation in pitching moment at off-design conditions. Perhaps the most severe limitation of the hodograph methods is that they cannot be readily extended to the design of three-dimensional wings where favorable two-dimensional characteristics are often degraded by the effects of wing sweepback and taper.

The disadvantages of the hodograph technique can be overcome by developing an airfoil design method to determine the flowfield and profile shape corresponding to a specified surface pressure distribution in the physical plane. Both relaxation and time-dependent finite-difference schemes would be appropriate for this type of calculation, although relaxation methods are preferable because of their increased speed.

This paper describes the application of generalized relaxation procedures to develop a method for designing efficient transonic airfoils and for modifying existing profiles. The inverse method is described in Sec. II, and the choice of an appropriate differencing scheme for the boundary conditions is discussed in Sec. III. Illustration of the design procedure is given in Sec. IV, and results of computations for several airfoil sections and for a simple three-dimensional wing are presented.

II. Formulation of the Design Procedure

Because one of the goals of the present investigation is to develop a method for designing airfoils containing weak shock waves, the flow can be assumed to be everywhere irrotational. With this approximation, the governing differential equations can be written in conservative form as

$$\partial F/\partial x + \partial G/\partial y = \quad \text{continuity} \tag{1}$$

$$\partial u/\partial y - \partial v/\partial x = 0 \quad \text{vorticity} \tag{2}$$

If the transonic small-disturbance approximation is made

$$F = \left[(1-M_\infty{}^2)(u-q_\infty) - \frac{\gamma+1}{2}M_\infty{}^2(u-q_\infty)^2\right] \qquad G = v \tag{3}$$

where u and v are x, y velocity components. If the complete compressible irrotational equations are used

$$F = \rho u/\rho_0 = G = \rho v/\rho_0$$

$$\frac{\rho}{\rho_0} = \left[1 - \frac{\gamma-1}{2}\left(\frac{u^2+v^2}{a_0{}^2}\right)\right]^{1/(\gamma-1)} \tag{4}$$

where ρ is the fluid density and a_0 is the speed of sound at stagnation. The details of the appropriate relaxation schemes for these systems of equations are described in the Appendix. Inverse calculations for flows with embedded shock waves are facilitated by solving the two coupled, first-order differential equations for the velocity components because of the ease in maintaining numerical consistency between direct and inverse problems (see Sec. III).

In the present, essentially preliminary study, the small-

Presented as Paper 72-679 at the AIAA 5th Fluid and Plasma Dynamics Conference, Boston, Mass., June 26–28, 1972; submitted July 27, 1972; revision received December 26, 1972.

Index category: Subsonic and Transonic Flow.

* Research Scientist. Member AIAA.

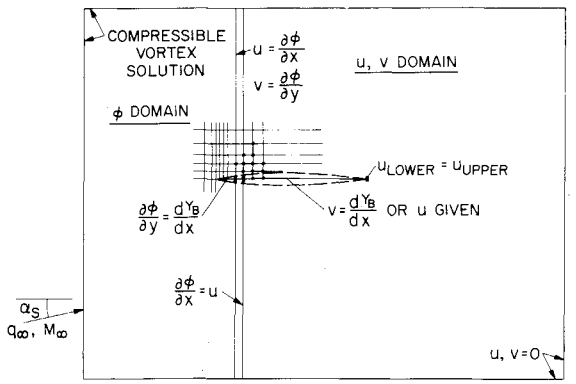

Fig. 1 Sketch of field subdivision.

disturbance approximation Eq. (3) and thin-airfoil boundary conditions are assumed. The use of Eq. (4) is preferable, but one of the difficulties associated with the full equations is that boundary conditions are usually applied on the airfoil surface, which itself is determined as part of the solution. Thin-airfoil theory, on the other hand, introduces a singularity at the profile leading edge that is difficult to resolve with the u, v relaxation procedure. The singularity can be effectively ignored in the numerical scheme for the velocity potential equation, however, as shown by Murman and Cole.[5] For this reason, a potential function is defined for the region between the upstream boundary and a line of mesh points just downstream of the leading edge. The velocity-component formulation is used in the remainder of the flowfield (Fig. 1). The first several points on the airfoil surface are therefore specified as a direct problem, and the design method is restricted to modifying the profile shape for a given nose geometry. One of the advantages of this procedure is that the large flow gradients in the vicinity of the leading edge are determined by the direct solution and need not be specified. Also, the subsequent integration of the streamline slopes to determine the airfoil coordinates can be initiated at a well-defined value and is therefore more accurate.

The design procedure formulated in this investigation is best suited to the modification of existing airfoil sections, although it is not limited to this application. Starting with a given profile—preferably one that can be closely approximated by thin-airfoil boundary conditions—a direct calculation is performed at either design or off-design Mach number and angle of attack. The airfoil coordinates in the vicinity of the leading edge are fixed, although the pressure is allowed to vary, with the physical extent depending on the grid spacing used (Fig. 1). A new pressure distribution that may contain weaker shock waves and improved lift and moment characteristics is subsequently specified over the remaining portion of the profile. Of course, not very specified pressure distribution results in a practical design, and usually an airfoil with either a blunt base or a nonphysical crossed trailing edge (negative thickness) is generated. As a result, an effective iteration procedure must be employed. The one used in the present method is to alternate between specifying the pressure distribution and the airfoil coordinates to obtain the desired profile shape. Several examples of this approach using a sequence of inverse and direct calculations are presented in Sec. IV.

III. Numerical Treatment of Boundary Conditions

An important requirement for any finite-difference design method, especially one that allows alternating between inverse and direct computations, is for the two procedures to be entirely consistent; e.g., if a pressure distribution containing a shock jump is computed for a given smooth airfoil section, the identical smooth airfoil section should be recovered when that discontinuous pressure distribution is specified and the airfoil shape recomputed. Since the same finite-difference approximations are used for all the field points in both the direct and inverse methods, only the differencing at the boundaries need be given critical examination. Selection of proper differencing schemes for the boundary conditions is described in this section.

Consider first a finite-difference method for the boundary in a direct calculation. Along the body, v is specified and values of u are unknown. However, for the method used to difference the interior points, u must be given at the boundary. This is accomplished by satisfying the vorticity equation along the body, combining an extrapolation scheme for the derivative $\partial u/\partial y$ with the given value of $\partial v/\partial x$; e.g., along the upper surface, the following differencing is used:

$$\partial u/\partial y|_{j,k} = (1/2\Delta y)(-3u_{j,k}+4u_{j,k+1}-u_{j,k+2}) = (\partial v/\partial x)_{j,k} = (d^2/dx^2)(Y_B(x)) \quad (5a)$$

where $Y_B(x)$ is the function that describes the body. Values of u_{jk} along the chord are then relaxed using the point Jacobi technique, which results in

$$u_{j,k} = \tfrac{4}{3}u_{j,k+1} - \tfrac{1}{3}u_{j,k+2} - [(2\Delta y/3)][d^2Y_B(x)/dx^2] \quad (5b)$$

In the inverse problem, values of v along the surface must be determined from the specified u distribution. This can be accomplished by again satisfying the vorticity relation, Eq. (5a), in which u_{jk} is specified and improved estimates for $u_{j,k+1}$ and $u_{j,k+2}$ are obtained as the field converges. The values of v can be found using either quadrature or differencing formulas. For either case, in the present method, the values of v_{jk} are calculated by performing the integration after each complete relaxation sweep of all interior field points.

The following differencing scheme is particularly efficient for subsonic flows. The value of $\partial v/\partial x$ in Eq. (5a) is approximated using third-order accurate difference formulas

$$\partial v/\partial x|_{j,k} = (1/6\Delta x)(-2v_{j-1,k}-3v_{j,k}+6v_{j+1,k}-v_{j+2,k}) \quad (6a)$$

for $j = 2, 4, 6, \ldots$, and

$$\partial v/\partial x|_{j,k} = (1/6\Delta x)(v_{j-2,k}-6v_{j-1,k}+3v_{j,k}+2v_{j+1,k}) \quad (6b)$$

for $j = 3, 5.7 \ldots$. The initial values of $v_{j-1,k}$ and $v_{j-2,k}$ are obtained from the specified profile shape near the leading edge. The relaxation scheme

$$v_{j,k}^{(n+1)} = v_{j,k}^{(n)} + \omega(-\partial u/\partial y + \partial v/\partial x)|_{j+1,k}$$
$$v_{j+1,k}^{(n+1)} = v_{j,k}^{(n)} - \omega(-\partial u/\partial y + \partial v/\partial x)|_{j,k}$$

for $k = 2, 4, 6 \ldots$ is then used to converge the body points. This differencing scheme proved accurate and efficient for subsonic flows but, unfortunately, is occasionally unstable for mixed, transonic flowfields. As a result, the quadrature formula described below was used for the inverse calculations presented in this paper.

In the quadrature approximation the simple trapezoidal rule is used, giving the relation

$$v_{j,k} = v_{j-1,k} + (\Delta x/2)[(\partial u/\partial y)_{j-1,k} + \partial u/\partial y|_{j,k}] \quad (7)$$

where $\partial u/\partial y$ is approximated by the same scheme used in Eq. (5). Because the distribution of v and $\partial v/\partial x$ is continuous and gradual, except possibly in the immediate vicinity of the nose of the airfoil (where they are given), Eq. (7) has proved sufficiently accurate for the present applications.

To verify the accuracy of the inverse method, the computations were performed on a variably spaced mesh of moderate size, 62×62, with the airfoil approximately at the center. (Typical results of a direct calculation for this grid are shown and compared to experiment in Fig. 2.) The surface pressure distribution obtained from a direct solution was used as a boundary condition for an inverse computation. The remaining flowfield was strongly perturbed from that given by the converged direct solution and used as the initial condition. The inverse solution was then relaxed to convergence and the values of v along the body were recovered to within ± 0.0005 of the originally specified body slope, with the exception of the last two mesh points upstream of the trailing-edge singularity. A comparison

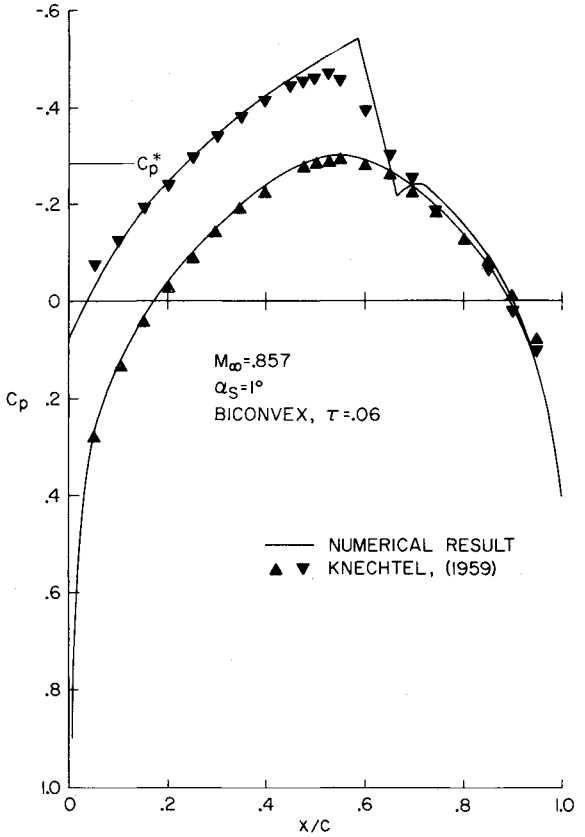

Fig. 2 Hybrid ϕ-uv solution for biconvex airfoil compared to experimental data.

between the specified and recomputed normal velocities is shown in Fig. 3 for the upper surface of a profile with an embedded shock wave. Similar results were obtained throughout the flowfield.

Using the vorticity equation for the boundary conditions of both the direct and inverse equations leads to an accurate reversible procedure. The values of v along the body could also be obtained by differencing the continuity equation, i.e.,

$$(1/2\Delta y)(-3v_{j,k}+4v_{j,k+1}-v_{j,k+2}) = \frac{\partial}{\partial x}[(1-M_\infty{}^2)(u-q_\infty)-(\gamma+1/2)M_\infty{}^2(u-q_\infty)^2]$$

where v_{jk} is determined during the relaxation process. In practice, however, this scheme was found to accumulate numerical error, probably because differencing across the shock wave is required. The discrepancy is evident as a slight discontinuity in v near the shock, and for a sequence of direct and inverse calculations, the error could become appreciable.

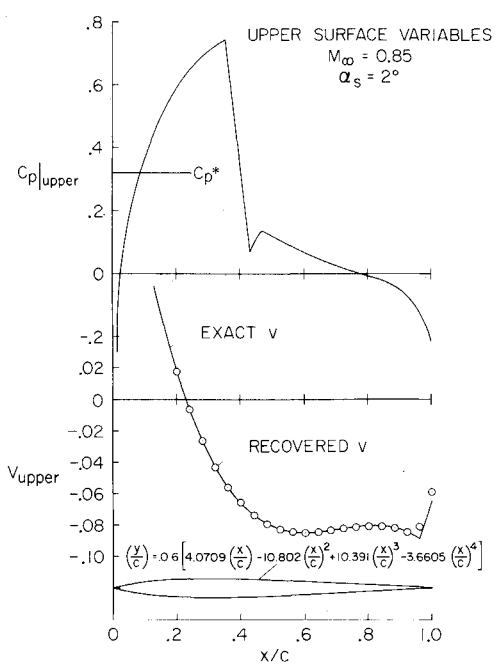

Fig. 3 Example of inverse verification calculation.

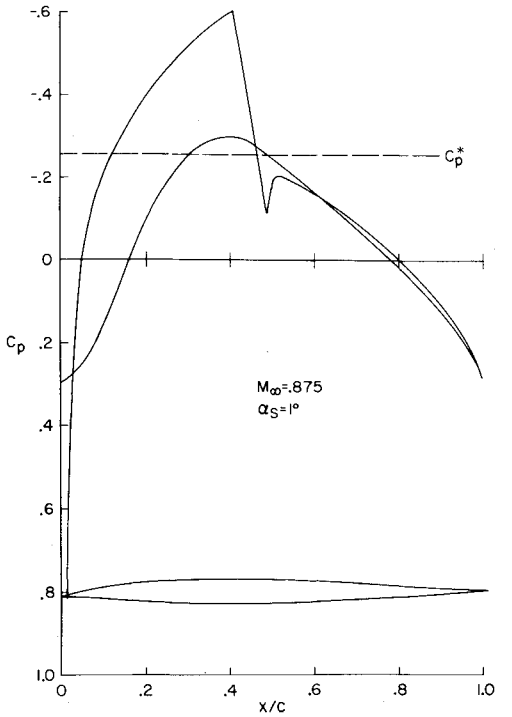

Fig. 4 Base airfoil.

IV. Results and Discussion

The results of a series of calculations are presented to illustrate the use of the finite-difference design method and to indicate possible extensions of the procedure. No particular attempt has been made to develop practical airfoil sections satisfying specific criteria.

A. Supercritical Airfoil Design

The following example was selected to illustrate the combination of inverse and direct procedures to extensively redesign an airfoil section. The calculations were performed dynamically, with all pressure and profile modifications input directly to the computer through an interactive graphics system.

The design sequence started with a direct calculation for an algebraically defined profile (Fig. 4). The airfoil has a sharp, cambered leading edge and is 6% thick, with maximum thickness located at the 40% chord. The nominal flow conditions for the airfoil were selected as 1° angle of attack at a relatively high freestream Mach number, $M_\infty = 0.875$. A moderate grid spacing was used, and the first 8% of the profile was in the region described by the velocity-potential equation and was not modified.

For the first design change (Fig. 5), the shock wave was reduced in strength and moved aft along the airfoil from 45 to

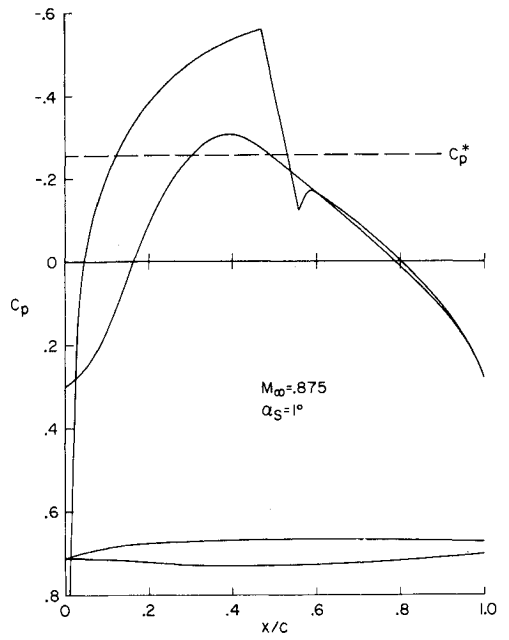

Fig. 5 Modification to weaken shock.

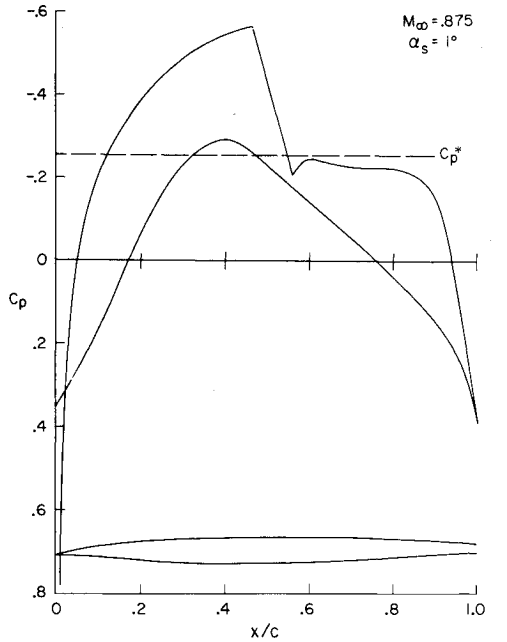

Fig. 6 Addition of sonic plateau.

52% chord to retain lift. The weakening of the shock strength decreased the curvature of the upper surface and resulted in a blunt-based airfoil. Most of the thickening was confined to the upper surface, although the curvature of the rear portion of the lower surface was also modified.

As the next step in the design process, a direct calculation was made for which a portion of the profile was removed from both the upper and lower surfaces near the trailing edge. The direct computation was not converged, but was run long enough to indicate the effect of this modification. A new pressure distribution, incorporating some of the properties of the direct solution was then specified. This distribution (Fig. 6) included a pressure plateau downstream of the shock wave to improve lift and to prevent the shock from growing in strength at off-design conditions. The resulting airfoil is also shown in Fig. 6. The rear portion of the profile is not as thick as that of the previous one, and the airfoil has acquired a slight reflexed camber on the lower surface.

With the upper surface tentatively designed, the lower surface was then modified to ensure airfoil closure, and a direct calculation was performed. During this phase of the iteration sequence, modifications to the lower surface altered the upper-surface pressure distribution. The changes were not large, and although it would have been possible to start again from a previous solution this option was not taken. The direct calculations also produced undesirable flow expansions near the trailing edge than were subsequently eliminated by respecifying the pressure. The new pressure distribution and the associated airfoil shape are shown in Fig. 7.

The profile design was terminated with a series of inverse calculations that resulted in the airfoil section and pressure distribution shown in Fig. 8. The supersonic velocities on the lower surface were eliminated, while all other changes were made to reduce the trailing-edge thickness. The final airfoil has less wave drag than the original profile and twice the lift coefficient. This is proabably not a practical design, however, because of the steep pressure gradients and high loading that exist at the rear of the airfoil.

B. Minor Airfoil Modification

The preceding example was provided to illustrate an interactive calculation resulting in an essentially new profile. A more straightforward application of the present method is to make minor refinements to an existing airfoil section that already satisfies certain design criteria. A simple example of the use of the inverse procedure for this purpose is shown in Fig. 9. For this calculation, the pressure plateau downstream of the shock on the upper surface was raised to the sonic value. The lift of the airfoil was increased by 10% with only a very slight modification of the profile shape.

C. Blunt-Nosed Airfoil Design

As previously discussed, the present method is based on the approximations of thin airfoil theory and is primarily applicable

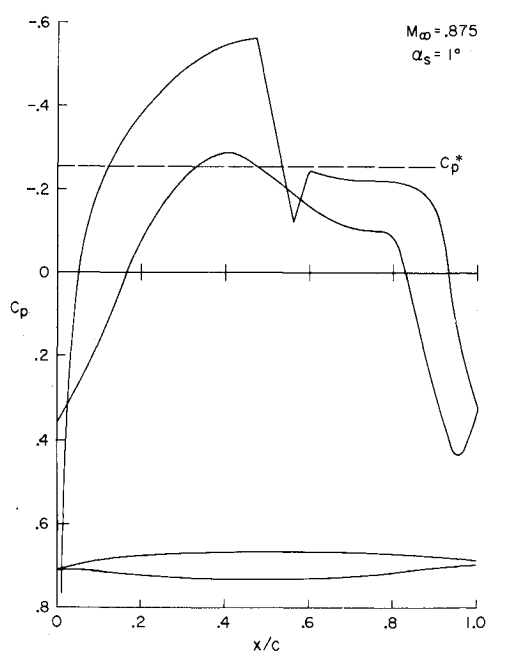

Fig. 7 Lower surface modification for closure.

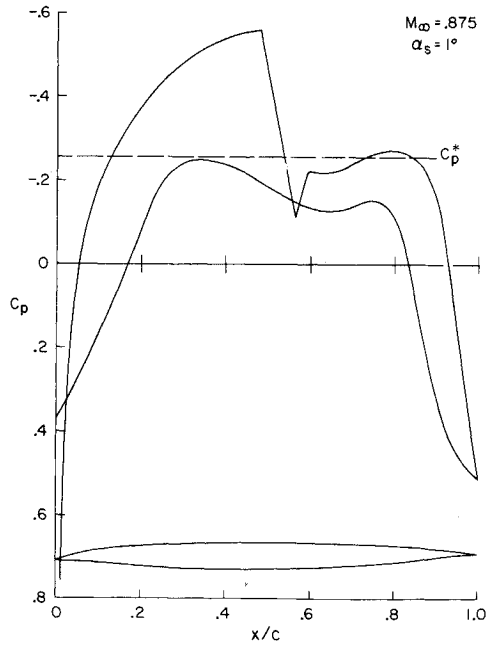

Fig. 8 Final design.

to thin, sharp-nosed profiles. With sufficient mesh refinement, however, it is possible to model blunt-nosed airfoils in the manner described by Murman and Krupp.[6,7] Even with a coarse mesh, the existing computer program can be used to suggest design modifications under the assumption that relative changes are accurately predicted. As an example of this application, an NACA 0010 profile at $M_\infty = 0.65$ and $\alpha = 2°$ was redesigned to increase lift. The lower-surface pressures of the original airfoil were accurately predicted, although the peak pressure coefficients on the upper surface were underestimated by as much as 20% at $x/c = 0.05$. This pressure distribution is compared to the solution for the modified airfoil in Fig. 10. Experience with this design and with other blunt-nosed airfoils indicates that these profiles are considerably easier to modify and properly close than airfoils with sharp leading edges.

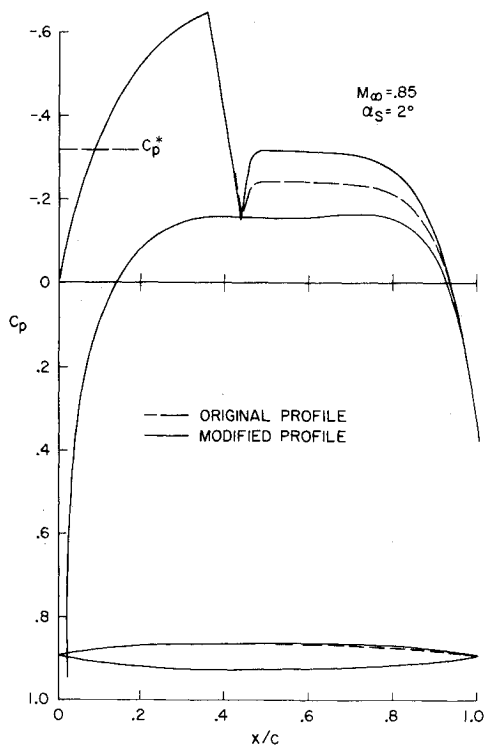

Fig. 9 Example of improving lift.

D. Shock-Free Designs

In addition to reducing shock strength to decrease wave drag, a shock-free surfuce pressure distribution can be specified. Unlike hodograph methods, however, there is no guarantee that imposing an arbitrary isentropic recompression at the airfoil surface will prevent a shock wave from forming in the field. This situation is illustrated in Fig. 11. Figure 11a shows the smooth, supercritical pressure distribution that was specified for both the upper and lower surfaces of an airfoil section. The profile shape and the sonic boundaries are shown in Fig. 11b. Flowfield pressure distributions showed that a shock wave formed above the upper surface at a height of approximately one body thickness, whereas the lower flowfield remained shock free. Both surfaces contain small supersonic compression ramps blended into the body to accommodate the specified smooth recompression. The reduction in curvature of the upper surface, however, was not sufficient to eliminate the shock formed by the reflections of leading-edge expansion waves from the sonic line.

E. Three-Dimensional Calculations

The extension of the present method to three dimensions is straightforward, although computation times increase with the number of mesh points. As demonstrated in Ref. 8 for direct calculations, values of u and w (here the normal z component) are supplied along the wing boundary by differencing two of the vorticity equations

$$\partial u/\partial z - \partial w/\partial x = 0$$
$$\partial v/\partial z - \partial w/\partial y = 0$$

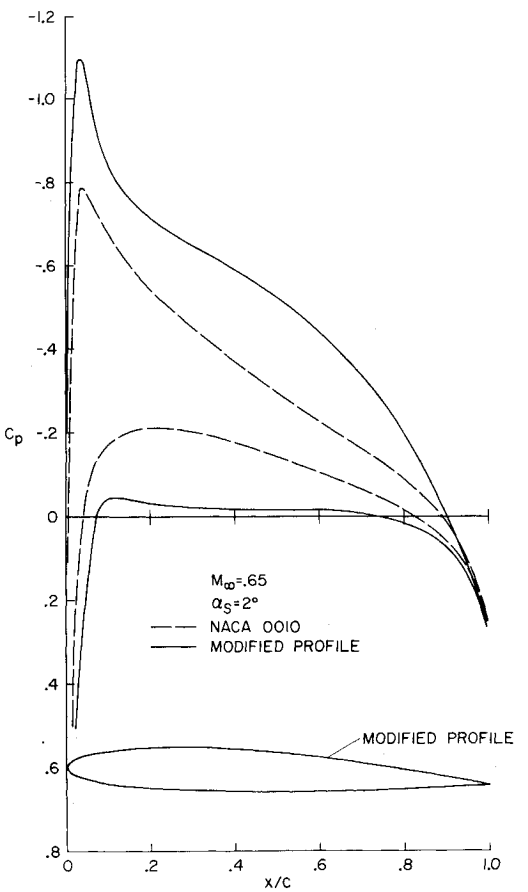

Fig. 10 Modification of 4-digit airfoil.

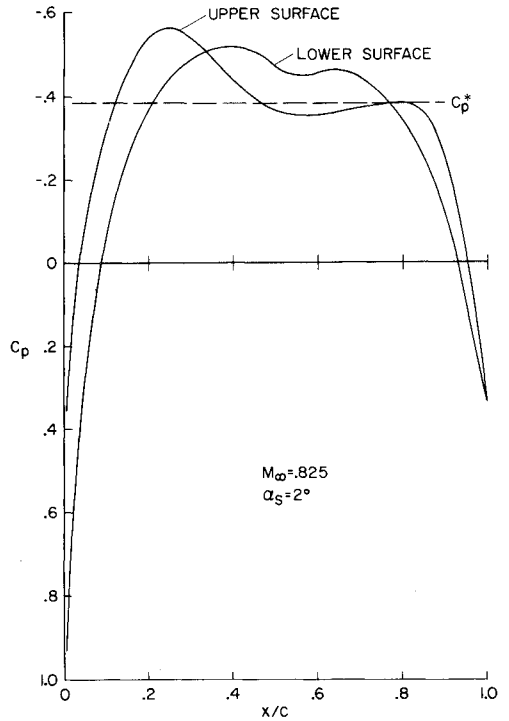

Fig. 11a Specified shock-free surface pressures.

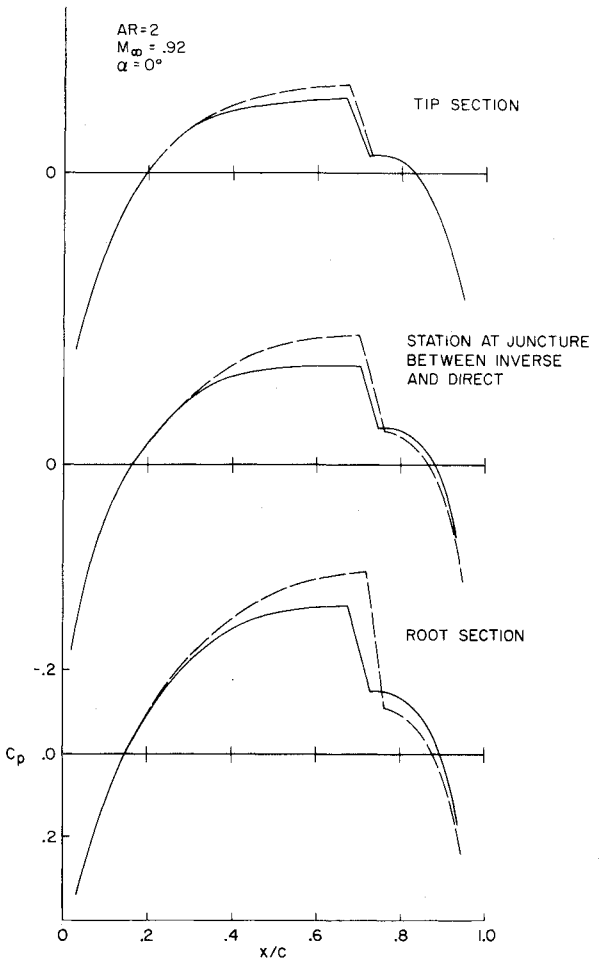

Fig. 12a Modified pressure compared to pressures of 6% thick biconvex wing.

For the inverse calculation, u is specified at the body and values of w are computed by exactly the same procedure used for the two-dimensional solution (see Sec. III).

Although no final three-dimensional wing designs have yet been completed, calculations to verify the stability of the inverse method have been performed on a coarse mesh. An example of this application is shown in Fig. 12 for a nonlifting, biconvex wing. For this calculation, the velocity-component formulation was used throughout the flowfield with a modified pressure distribution specified over the inboard section of the wing. As a first step in a possible iteration sequence, the strength of the shock wave was decreased, resulting in a typical reduction in curvature and the formation of a blunt trailing edge.

V. Conclusions

The present paper has described a preliminary method for designing transonic airfoil sections and for modifying existing profiles. Several examples of inverse calculations have been presented to illustrate various applications and limitations of the procedure. The most important disadvantage of the present method is that the use of the small-disturbance approximation with thin-airfoil boundary conditions makes it difficult to obtain accurate solutions for the practical case of blunt-nosed lifting airfoils. Modification of the design procedure developed in this investigation to solve the full equations for more complicated geometries is straightforward, however. Because the present method incorporates alternate inverse and direct computations, it would be necessary to adjust the body coordinate system during the direct portions of the calculation only. As the final

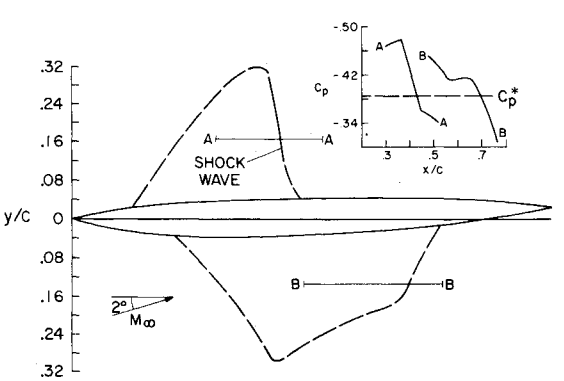

Fig. 11b Profile computed from specified shock-free surface pressures.

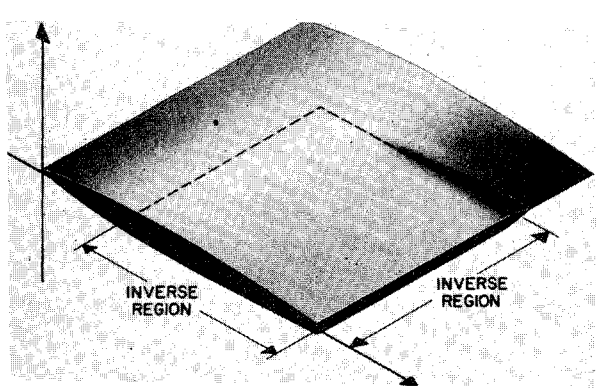

Fig. 12b Sketch of modified wing showing inverse region.

design evolved, changes in the profile shape would become minor and the boundary conditions would automatically be specified along the airfoil surface.

Appendix

The relaxation scheme developed for the primitive variables has been described in Refs. 8 and 9. Several extensions to the method have recently been completed and are outlined in this Appendix.

A. Finite-Difference Operators

Although a variable mesh was used for the results presented in the text for simplicity, the difference formulas are written here for a uniform mesh. Representing F or $-v$ by f, and G or u by g, the y derivatives of both Eqs. (1) and (2) are approximated by the difference operators

$$\partial g/\partial y|_{j,k} = (1/2\Delta y)(-3g_{j,k}+4g_{j,k+1}-g_{j,k+2})+ 0\{[(\Delta y/)^2/3]g'''_{j,k}\}, \quad k=2,4,6,\ldots,KM-2 \qquad \text{(A1a)}$$

and

$$\partial g/\partial y|_{j,k} = (1/2\Delta y)(3g_{j,k}-4g_{j,k-1}+g_{j,k-2})+ 0\{[(\Delta y)^2/3]g'''_{j,k}\}, \quad k=3,5,7,\ldots,KM-1 \qquad \text{(A1b)}$$

where 1 and KM are end points and for convenience KM is usually an even index. In regions of subsonic flow, the x derivatives are approximated by central differencing

$$\partial f/\partial x|_{j,k} = (1/2\Delta x)(f_{j+1,k}-f_{j-1,k})-0\{[(\Delta x)^2/6]f'_{j,k}\} \qquad \text{(A2)}$$

and for supersonic flow,

$$\partial f/\partial x|_{j,k} = (1/4\Delta x)(3f_{j,k}-4f_{j-2,k}+f_{j-4,k})+ 0[\tfrac{4}{3}(\Delta y)^2 f'''_{j,k}] \qquad \text{(A3)}$$

Here the usual three-point backward differencing has been written for a spacing of $2(\Delta x)$ because the conventional single spacing leads to an unstable iteration scheme. Note that the equations are differenced in conservative form and are second-order accurate. In practice, a linear combination of the x difference analogs is used over an interval defined by $0.98\rho^* \leqq \rho \leqq \rho^*$ to avoid a sudden change of data utilization during the iteration process.

Because the x derivatives employ a weighting of every other point, it is possible for the variables at, e.g., odd indexed j-points to become uncoupled from the variables at even indexed j-points. In the vicinity of the shock or near discontinuous boundaries, the iteration scheme for the nonlinear equations can become unstable. For this reason coupling terms are added to the difference equations. The quantity

$$\delta_{j,k} = \varepsilon(g_{j+1,k}-2g_{j,k}+g_{j-1,k})-\varepsilon 0[(\Delta x)^2 g''_{j,k}]$$

is added in subsonic regions, and

$$\delta_{j,k} = \varepsilon(-g_{j,k}+2g_{j-1,k}-g_{j-2,k})+\varepsilon 0[(\Delta x)^2 g''_{j,k}]$$

is included for supersonic regions. The term ε is less than 1 and is small compared to $1/2\Delta x$. The $\delta_{j,k}$ are not needed as dissipation terms and in subsonic flow, for points away from discontinuities, they may be discarded if Eq. (A2) is replaced by a properly coupled operator such as

$$\partial f/\partial x|_{j,k} = (1/12\Delta x)(f_{j-2,k}-8f_{j-1,k}+8f_{j+1,k}-f_{j+2,k})+ 0\{[(\Delta x)^4/30]f'''''_{j,k}\} \qquad \text{(A4)}$$

This equation is fourth-order accurate. If consistent accuracy is desired for the y differencing, Eq. (A1) could be replaced by Eq. (6).

B. Interchange Relaxation Algorithm

Define

$$g' = \Delta f/\Delta x + \Delta g/\Delta y \qquad \text{(A5)}$$

where $\Delta f/\Delta x$ and $\Delta g/\Delta y$ represent the previously described difference analogs to the partial derivatives, Eqs. (A1–4). The iteration process for the difference equations is defined by

$$g^{(n+1)}_{j,k} = g^{(n)}_{j,k}+\omega(g'^{(n,n+1)}_{j,k+1}+\delta^{(n,n+1)}_{j,k}) \qquad \text{(A6a)}$$

$$g^{(n+1)}_{j,k+1} = g^{(n)}_{j,k+1}-\omega(g'^{(n,n+1)}_{j,k}-\delta^{(n,n+1)}_{j,k+1}) \qquad \text{(A6b)}$$

where $k=2,4,6,\ldots,KM-2$. This algorithm describes a successive point scheme for Eqs. (1) and (2) which has convergence rates equivalent to successive overrelaxation schemes developed for the potential equation when $\Delta x = \Delta y$. Note that the $\delta_{j,k}$ coupling term corresponds to an adjacent point in the y direction and is alternately added and subtracted in the difference equation.

More rapid convergence can be obtained with line relaxation, and the interchange algorithm is readily adapted to this mode of iteration. Along a row of vertical points the y difference operator defined by Eqs. (A1) generates the system of equations

$$\begin{bmatrix} \Delta g/\Delta y|_{j,k} \\ \Delta g/\Delta y|_{j,k+1} \\ \Delta g/\Delta y|_{j,k+2} \\ \Delta g/\Delta y|_{j,k+3} \end{bmatrix} = \frac{1}{2\Delta y} \begin{bmatrix} \cdot & \cdot & \cdot & \cdot & \cdot & \cdot \\ \cdot & -3 & 4 & -1 & 0 & \cdot \\ \cdot & -4 & 3 & 0 & 0 & \cdot \\ \cdot & 0 & 0 & -3 & 4 & \cdot \\ \cdot & 0 & 1 & -4 & 3 & \cdot \\ \cdot & \cdot & \cdot & \cdot & \cdot & \cdot \end{bmatrix} \begin{bmatrix} g_{j,k} \\ g_{j,k+1} \\ g_{j,k+2} \\ g_{j,k+3} \end{bmatrix}$$

Applying the interchange algorithm, this same block of difference equations assumes a tridiagonal, diagonally dominant form

$$\begin{bmatrix} \Delta g/\Delta y|_{j,k+1} \\ -\Delta g/\Delta y|_{j,k} \\ \Delta g/\Delta y|_{j,k+3} \\ -\Delta g/\Delta y|_{j,k+2} \end{bmatrix} = \frac{1}{2\Delta y} \begin{bmatrix} \cdot & \cdot & \cdot & \cdot & \cdot & \cdot \\ \cdot & -4 & 3 & 0 & 0 & \cdot \\ \cdot & 3 & -4 & 1 & 0 & \cdot \\ \cdot & 0 & 1 & -4 & 3 & \cdot \\ \cdot & 0 & 0 & 3 & -4 & \cdot \\ \cdot & \cdot & \cdot & \cdot & \cdot & \cdot \end{bmatrix} \begin{bmatrix} \cdot \\ g_{j,k} \\ g_{j,k+1} \\ g_{j,k+2} \\ g_{j,k+3} \\ \cdot \end{bmatrix}$$

These tridiagonal blocks are readily inverted and can be included in the line relaxation scheme in the usual fashion. For this scheme, a typical relaxation factor, ω, has a value of 0.4 when $\Delta x = \Delta y$ and is directly proportional to the ratio of step sizes, $\Delta x/\Delta y$. The efficiency of the method is therefore poor if $\Delta x \ll \Delta y$, and such grids must be avoided. In contrast to schemes that have been developed for the potential equation, convergence is not degraded if the grid is swept from downstream to upstream during the relaxation, and the direction of the sweep can alternate with each iteration.

C. Complete Irrotational, Compressible Equations

The results shown in this paper used the transonic small-perturbation equations, but the identical procedure applies to Eqs. (4). Values of G and u are obtained directly from the interchange scheme for these complete equations. Updated estimates for $(\rho/\rho_0)^{(n+1)}$ are found from the energy equation, which, for purposes of computer efficiency, is approximated by a truncated binomial series. The full equations require only slightly more algebra than the transonic small-perturbation equations. The number of difference operators is the same and the same tridiagonal inversion routine is used.

References

[1] Nieuwland, G. Y., "Transonic Potential Flow Around a Family of Quasi-elliptical Aerofoil Sections," NLR-TR T.172, 1967, National Lucht-en Ruimtevaart-Laboratorium, Amsterdam.

[2] Boerstoel, J. W. and Uijlenhoet, R., "Lifting Aerofoils with Supercritical Shockless Flow," ICAS Paper 70-15, 1970, International Council of the Aerospace Sciences.

[3] Garabedian, P. R. and Korn, D. G., "Numerical Design of Transonic Airfoils," *Numerical Solution of Partial Differential Equations—II*, Academic Press, New York, 1971.

[4] Kacprzynski, J. J., Ohman, L. H., Garabedian, P. R., and Korn, D. G., "Analysis of the Flow Past the Shockless Lifting Airfoil in Design and Off-Design Conditions," AIAA Paper 71-567, Palo Alto, Calif., 1971.

[5] Murman, E. M. and Cole, J. D., "Calculation of Plane Steady Transonic Flows," *AIAA Journal*, Vol. 9, No. 1, Jan. 1971, pp. 114–121.

[6] Krupp, J. A. and Murman, E. M., "The Numerical Calculation of Steady Transonic Flows Past Thin Lifting Airfoils and Slender Bodies," AIAA Paper 71-566, Palo Alto, Calif., 1971.

[7] Murman, E. M. and Krupp, J. A., "Solution of the Transonic Potential Equation Using a Mixed Finite Difference System," *Lecture Notes in Physics*, Vol. 8, Springer-Verlag, Berlin, 1971.

[8] Bailey, F. R. and Steger, J. L., "Relaxation Techniques for Three-Dimensional Transonic Flow About Wings," AIAA Paper 72-189, San Diego, Calif., 1972.

[9] Steger, J. L. and Lomax, H., "Generalized Relaxation Methods Applied to Problems in Transonic Flow," *Lecture Notes in Physics*, Vol. 8, Springer-Verlag, Berlin, 1971.

Experimental Determination of the Aeroacoustic Environment about a Slender Cone

A. MARTELLUCCI,* L. CHAUMP,† AND D. ROGERS‡
General Electric Company, Philadelphia, Pa.

AND

D. SMITH§
Wright-Patterson Air Force Base, Ohio

Acoustic pressure fluctuation and heat-transfer data have been obtained on a 7.2° half-angle cone. Measurements were obtained at Mach 4, 8, and 10 for several values of the freestream Reynolds number and cone angle of attack, and three bluntness ratios. Natural transition was achieved in all cases. Methods of data acquisition and analysis are discussed. Selected boundary-layer root-mean-square (rms) pressure fluctuation data and transition front shape, deduced from the heat-transfer data, are presented. Heat transfer, rms pressure, and turbulent velocity profile exponent data are all shown to peak near the end of transition.

Nomenclature

C_f = skin-friction coefficient
db = decibel (reference pressure 0.0002 μbars)
E = end of transition (peak $\dot{q}$)
H_0, h_w = stagnation and wall enthalpy, respectively
L = model length
M = Mach number
n = velocity profile exponent
0 = onset of transition (minimum $\dot{q}$)
$\tilde{P}$ = rms fluctuating pressure
q = dynamic pressure
$\dot{q}$ = heat-transfer rate
R = radius
Re/ft = unit Reynolds number per foot
Re_s = local wetted length Reynolds number
S = wetted length along cone
S_T = Stanton number
T = temperature
u = axial velocity
x = axial coordinate
y = coordinate normal to surface
α = angle of attack
δ = boundary-layer thickness
γ = ratio of specific heats
θ_c = cone half angle
μ = molecular viscosity
ρ = density

Subscripts

aw = adiabatic wall
B = model base
e = edge of boundary layer
L = edge of laminar sublayer
N = nose
T = transition onset
w = conditions at wall
∞ = freestream conditions

Presented as Paper 72-706 at the AIAA 5th Fluid and Plasma Dynamics Conference, Boston, Mass., June 26–28, 1972; received August 7, 1972; revision received November 27, 1972. This research was sponsored by the Air Force Flight Dynamics Laboratory (AFFDL), Wright-Patterson Air Force Base, Ohio under contract F33615-71-C-1245. The authors wish to acknowledge the efforts of F. George and C. Davies for their assistance in fabrication and assembly of the model, and to A. Monfort for his contribution in the data analysis and evaluation.

Index categories: Supersonic and Hypersonic Flow; Boundary-Layer Stability and Transition.

* Consultant, Aerothermodynamics Laboratory. Associate Fellow AIAA.

† Manager, Structural Mechanics Laboratory. Member AIAA.

‡ Supervising Engineer—Instrumentation. Member AIAA.

§ Project Engineer, Air Force Flight Dynamics Laboratory.

I. Introduction

DURING re-entry into the Earth's atmosphere, vehicles are subjected to intense fluctuating aerodynamic pressures. As a result, significant vibration response can occur affecting the performance of components within the vehicle. In order to accurately assess this problem, it is necessary to define the nature of the acoustic environment associated with turbulent flow over the re-entry vehicle. This has become more important as mission requirements have resulted in higher velocities at relatively lower altitudes. Predictions based on available low Mach number data indicate that sound pressure levels on the order of 190 db may be encountered.

The purpose of the program undertaken in the present study was to measure the aeroacoustic environment on the surface